Biophysical Journal
Article

Biophysical Society

Membrane Bending Moduli of Coexisting Liquid Phases Containing Transmembrane Peptide

Rebecca D. Usery,[1] Thais A. Enoki,[1] Sanjula P. Wickramasinghe,[1,2] V. P. Nguyen,[3] David G. Ackerman,[1,4] Denise V. Greathouse,[5] Roger E. Koeppe,[5] Francisco N. Barrera,[3] and Gerald W. Feigenson[1,*]
[1]Department of Molecular Biology and Genetics, Cornell University, Ithaca, New York; [2]Department of Biochemistry and Biophysics, University of Pennsylvania, Philadelphia, Pennsylvania; [3]Department of Biochemistry & Cellular and Molecular Biology, University of Tennessee, Knoxville, Tennessee; [4]Scientific Computing, Howard Hughes Medical Institute, Janelia Research Campus, Ashburn, Virginia; and [5]Department of Chemistry and Biochemistry, University of Arkansas, Fayetteville, Arkansas

ABSTRACT A number of highly curved membranes in vivo, such as epithelial cell microvilli, have the relatively high sphingolipid content associated with "raft-like" composition. Given the much lower bending energy measured for bilayers with "nonraft" low sphingomyelin and low cholesterol content, observing high curvature for presumably more rigid compositions seems counterintuitive. To understand this behavior, we measured membrane rigidity by fluctuation analysis of giant unilamellar vesicles. We found that including a transmembrane helical GWALP peptide increases the membrane bending modulus of the liquid-disordered (Ld) phase. We observed this increase at both low-cholesterol fraction and higher, more physiological cholesterol fraction. We find that simplified, commonly used Ld and liquid-ordered (Lo) phases are not representative of those that coexist. When Ld and Lo phases coexist, GWALP peptide favors the Ld phase with a partition coefficient of 3–10 depending on mixture composition. In model membranes at high cholesterol fractions, Ld phases with GWALP have greater bending moduli than the Lo phase that would coexist.

INTRODUCTION

Many cellular functions and structures require membrane deformation. For example, bending of the plasma membrane (PM) occurs in tubulation, fission, and fusion (1). In addition to transient membrane curvature in these processes, the membrane exhibits curvature extremes for structures such as microvilli, dendritic trees, small vesicles, and virus particles. Membrane lipids and associated protein components can be sorted by curvature in vitro; a less rigid lipid composition can more readily accommodate curvature, and proteins may prefer that curvature to varying extents (2,3).

As an intrinsic plasma-membrane-organizing principle, ordered, functional platforms or "membrane rafts" are thought to have roles in signaling, cytoskeletal attachment, and virus budding. This membrane compartmentalization can be studied in chemically simplified and compositionally well-defined model membranes. Mixtures of high-melting (high-Tm) lipids, low-melting (low-Tm) lipids, and cholesterol (chol) exhibit liquid-ordered (Lo) and liquid-disordered (Ld) phases, as well as Lo + Ld phase coexistence analogous to raft + nonraft behavior in cells (4–7). For coexisting Lo + Ld, domains are either microns or nanometers in diameter, termed macro- and nanoscopic phase separation, respectively. The rich-phase behavior of mixtures of this type, including the regions of Ld + Lo phase coexistence, has been mapped (4–12). Precise determination of phase boundaries and the critical point allow estimation of compositions of coexisting phases, connected in the phase diagram via tielines.

Rafts are thought to be more rigid than their nonraft counterparts because the Lo bending moduli are greater than those of Ld phases (2,13–15). More rigid membranes would bend less for a given applied force, yet many highly curved membranes have raft-like compositions. Even the first demonstrations of lipid-based organization showed that proportionally more glycosphingolipids sort to the apical side of epithelial cells, leading to a raft-like composition accommodating the extreme curvature of microvilli (16). Highly curved virus particles have raft-like composition (17), as do synaptosomes (18). Dendritic cells, considered to be "raft-rich," have fewer extensively branched dendritic trees with spines of larger diameter when sphingolipid synthesis and cholesterol synthesis are inhibited as a means to disrupt membrane rafts (19). Interaction with the actin cytoskeleton

Submitted January 4, 2018, and accepted for publication March 22, 2018.
*Correspondence: gwf3@cornell.edu
Editor: Kalina Hristova.
https://doi.org/10.1016/j.bpj.2018.03.026

dimples the membrane and is associated with raft formation (20). A variety of cancer cells reprogram to be more raft-rich (21) but are softer mechanically (22). Other factors are likely involved in each of these examples, but their number and diversity suggest a problem with the view of rafts as rigid platforms compared to the nonraft component.

This apparent difference between membrane bending rigidity in vitro and in vivo may be connected to the significant protein component in the membrane, a contribution neglected by lipid-only models. As a model for occupancy of the membrane interior by protein, we have used a model transmembrane helical peptide. The family of WALP-like peptides has been designed to resemble α-helical transmembrane segments of membrane proteins and has proven useful in the elucidation of peptide-lipid interaction principles (23,24). The peptides have a hydrophobic core of alternating leucine and alanine residues and have aromatic or charged residues at the ends of the peptide that prefer the aqueous membrane interface (25–27). Partial unwinding of the peptide terminals provides further stabilization at the membrane interface (28). As a single helix spanning the membrane, the WALP-like peptides are a useful model of single-pass proteins that account for ~40% of transmembrane domains and are thereby the most common transmembrane anchor (29,30). GWALP23 in particular was used in this study because previous NMR studies demonstrated that the peptide had a well-defined transmembrane orientation that exhibits modest dynamic averaging and is tilted from the bilayer normal in a manner that scales with the bilayer thickness in various single-component bilayers (27). The 23-residue length of GWALP23 is within the range of lengths observed for vertebrate plasma membrane transmembrane domains (31).

In this work, we have measured the bending moduli of Ld and Lo phases. We have compared commonly used, simplified one- and two-component models of Ld and Lo to three-component Ld and Lo phases that actually coexist. To know the compositions of coexisting phases, we begin with the most accurately determined thermodynamic tieline, which is the lower boundary of the two-phase liquid-liquid coexistence region. We prepare membranes of tieline endpoint compositions and independently measure the bending moduli of these phases that would coexist for four different ternary mixtures, including examples of both nanoscopic and macroscopic phase separation. We then investigate whether a model transmembrane helix affects phase behavior, how it partitions between Ld and Lo, how it is oriented in the bilayer, and how it affects bending moduli at relevant fractions. We have addressed these questions at a low-cholesterol fraction, at which the Ld and Lo phase compositions are most different, and also at a higher, more physiological cholesterol fraction. We find that the presence of a helical peptide causes the bending rigidity of the Ld phase to approach and, at physiological cholesterol concentrations, exceed that of the Lo phase. Our findings provide a potential explanation for the raft-like lipid composition of a number of highly curved membranes, as well as a reason to reconsider raft + nonraft behavior in cells.

MATERIALS AND METHODS

Materials

Brain sphingomyelin (bSM), 1,2-dioleoyl-sn-glycero-3-phosphocholine (DOPC), 1-palmitoyl-2-oleoyl-sn-glycero-3-phosphocholine (POPC), and 1,2-distearoyl-sn-glycero-3-phosphocholine (DSPC) were purchased from Avanti Polar Lipids (Alabaster, AL). Piperazine-N,N′-bis(2-ethanesulfonic acid)), potassium chloride, and ethylenediaminetetraacetic acid were obtained from Sigma-Aldrich (St. Louis, MO). Sucrose was from Fisher Scientific (Fair Lawn, NJ), and glucose from Teknova (Hollister, CA). The purity of phospholipids was found to be better than 99.5% using thin layer chromatography. Briefly, ~20 μg of lipid was spotted on washed and activated Adsorbosil TLC plates (Alltech, Deerfield, IL) and developed in chloroform/methanol/water = 65/25/4. Phospholipid concentrations were determined by inorganic phosphate assay (32), with an error <1% from 10 replicates. Cholesterol was from Nu Chek Prep (Elysian, MN), and stock solutions were made at defined concentrations using standard gravimetric procedures. The fluorescent dyes, 1,1′-didodecyl-3,3,3′,3′-tetramethylindocarbocyanine perchlorate (C12:0 DiI), benzoxazolium, 3-(9,12-octadecadienyl)-2-[3-[3-(9,12-octadecadienyl)-2(3H)-benzoxazolylidene]-1-propenyl]-, perchlorate (FAST DiO), and 2-(4,4-difluoro-5,7-dimethyl-4-bora-3a,4adiaza-s-indacene-3-pentanoyl)-1-hexadecanoyl-sn-glycero-3-phosphocholine (BODIPY-PC) were from Invitrogen (Carlsbad, CA). Tryptophan oleoyl ester (TOE) was synthesized in the laboratory of Erwin London, and ergosta-5,7,9 (11),22-tetraen-3β-ol (DHE) was from Sigma-Aldrich. Concentrations were determined by absorption spectroscopy using an extinction coefficient of 143,000 $M^{-1}cm^{-1}$ for C12:0 DiI, 153,000 $M^{-1}cm^{-1}$ for FAST DiO, 91,800 $M^{-1}cm^{-1}$ for BODIPY-PC, 5600 $M^{-1}cm^{-1}$ for TOE, and 12,900 $M^{-1}cm^{-1}$ for DHE. Spin-labeled lipid 1-palmitoyl-2-(16-doxyl stearoyl) phosphatidylcholine (16PC) and 1-palmitoyl-2-(7-doxyl stearoyl) phosphatidylcholine (7PC) were a gift from Boris Dzikovski of the National Biomedical Center for Advanced ESR Technology at Cornell University. $F^{4,5}$GWALP23 (acetyl-GGAFF $(LA)_6$LWLAGA-ethanolamide) (27), hereafter referred to as GWALP23, was synthesized and purified according to (26). The peptide was dissolved in 2,2,2-trifluorethanol from Sigma-Aldrich, with the peptide concentration measured by tryptophan absorbance at 280 nm using an extinction coefficient of 5600 $M^{-1}cm^{-1}$.

GUV preparation

Giant unilamellar vesicles (GUVs) were made by gentle hydration (33) to produce GUVs with uniformly low membrane tension without adding salt, often needed for electroswelled GUVs (13). Charged lipid provides repulsion between layers in the lipid films to improve hydration of the sample, so 2 mol% of the total lipid in each sample was replaced with the phosphatidylglycerol cognate of the major lipid. Each sample contained 250 nmol of a lipid or protein/lipid mixture in 200 μL of 2:1 chloroform: methanol. A thin, even film was created in the bottom of glass tubes using a rotary evaporator. During solvent evaporation, sample tubes were heated to above the transition temperatures of all lipid components, 45 or 55°C for bSM- or DSPC-containing mixtures, respectively. Residual solvent was then removed by vacuum pumping for 2 h at ~30 mTorr at room temperature. Films were hydrated with the temperature maintained above the transition temperature. GUVs were formed in sucrose solution as the films were cooled from above the transition temperature to 23°C over 12 h using a Digi-sense temperature controller R/S (Cole Palmer, Vernon Hills, IL). GUVs were harvested into glucose solution, then allowed to settle for 1 h to remove debris before microscopy observations. Experiments were

conducted using an inverted widefield microscope, a Nikon Eclipse Ti (Nikon Instruments, Melville, NY) equipped with a 60×/1.2 NA phase-contrast oil-immersion objective and Sola solid-state white-light-excitation source (Lumencor, Beaverton, OR), which was necessary to achieve sufficient contrast in short exposures for measuring bending moduli, particularly those of the Lo phases.

Membrane bending rigidity measurements

Bending moduli were measured as in (34) by fluctuation analysis of GUVs. Briefly, fluctuations at the GUV equator were observed by phase-contrast microscopy. Fluctuation spectra from GUV contours were used to calculate the bending modulus through the relationship

$$\left\langle |u(q)|^2 \right\rangle = \frac{k_B T}{\kappa q^4 + \sigma q^2}, \quad (1)$$

where $u(q)$ is the displacement normal to the membrane, $q = (qx, qy)$ is the wave vector corresponding to the displacement, k_B is the Boltzmann constant, T is the absolute temperature, κ is the bending modulus, and σ is membrane tension. All measurements were carried out at room temperature. The bending moduli of the coexisting phases were determined by measuring single-phase GUVs at the Ld and Lo tieline endpoint compositions. See Supporting Material for additional information on measurement methods.

FRET trajectories for phase boundaries and K_p determination

We prepared samples along a thermodynamic tieline by rapid solvent exchange (35) and measured Förster resonance energy transfer (FRET) at room temperature. Decreased FRET, as illustrated in Fig. 1, is observed in the two-phase region when donor and acceptor probes partition into different phases. Phase boundaries are identified from the FRET curve shape as previously described (5,7,11). Briefly, boundaries are defined by the intersection of linear fits in the regions neighboring an abrupt change in the FRET signal. An internal normalization in the FRET profiles was used to correct variations between samples, such as small differences in sample concentration (36). The fluorescence emission of the acceptor stimulated by the energy transfer of the donor, FRET, was normalized by the donor and acceptor emission in each sample.

K_p determinations were conducted as previously described (34). Briefly, along a tieline, the FRET signal of probes that equilibrate between two phases can be expressed as (36),

$$FRET = \frac{FL_D + \chi L_O\left(FL_O K_p^D K_p^A - FL_D\right)}{\left[1 + \left(K_p^D - 1\right)\chi L_O\right]\left[1 + \left(K_p^A - 1\right)\chi L_O\right]}, \quad (2)$$

where F_{Ld} and F_{Lo} are the intensities in Ld and Lo phases, χ_{Lo} is the phase fraction corresponding to Lo phase, K_p^D is the partition coefficient of the donor, and K_p^A is the partition coefficient of the acceptor. The fraction of Lo phase, χ_{Lo}, corresponds to the independent variable of Eq. 2. $K_p > 1$ refers to preference for the Ld phase here. For GWALP23 partition coefficient determination, we used FRET between the Trp residue of the peptide and DHE, a cholesterol analog. Cholesterol K_p is known from the phase diagrams for the mixtures used in this work (7,11). Experimental data were then fit to Eq. 2 with one free parameter, the peptide K_p. Emission and excitation wavelengths for these experiments are summarized in Tables S1 and S2.

Circular dichroism

Large unilamellar vesicles (LUVs) were prepared by extruding rapid solvent exchange samples using a miniextruder (Avanti Polar Lipids) assembled with a single polycarbonate filter of 100-nm-diameter pore size. Measurements were performed on a Jasco J-815 spectropolarimeter (Easton, MD) at 25°C with a scan rate of 100 nm/min and 25 accumulations. The peptide:lipid molar ratio was 1:50, with a final peptide concentration of 5 μM. Raw data were converted into mean residue ellipticity according to $[\Theta] = \Theta/(10lcN)$, where Θ is the measured ellipticity, l is

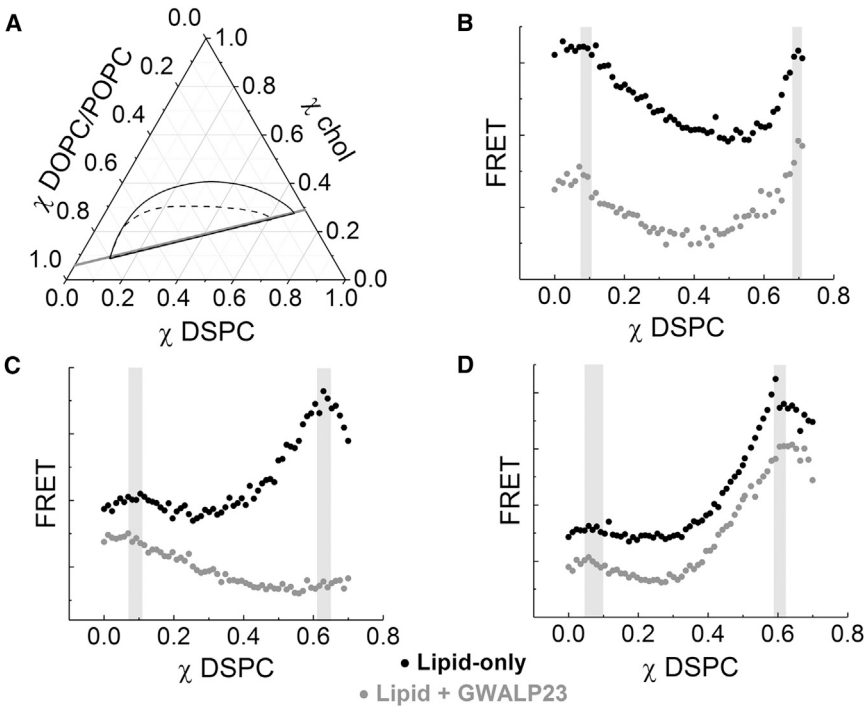

FIGURE 1 Presence of GWALP23 does not change phase boundaries. (*A*) The compositional trajectory (*gray line*) along which 70 samples were made and the phase coexistence region (Ld + Lo) for DSPC/DOPC/chol (*black outline*) and DSPC/POPC/chol (*dashed line*) at 23°C are shown, adapted from Ref. (7). (*B*) FRET from DHE to FAST DiO in DSPC/DOPC/chol along the trajectory in (*A*), in the absence and in the presence of 2 mol% GWALP23, is shown. The FRET intensity (in arbitrary units, AU) along the trajectory is shown in black for the lipid-only case and in gray in the presence of peptide (shifted lower for clarity). Phase boundaries correspond to the shaded regions. The width of each shaded region depicts the fitting error. (*C*) FRET trajectories using Trp and DHE in DSPC/POPC/chol for both the lipid-only trajectory (*black*), wherein the Trp is that of TOE, and the trajectory with 2 mol% GWALP23 (*gray*) are shown. (*D*) FRET trajectories using DHE and BODIPY-PC in DSPC/POPC/chol for both the lipid-only trajectory (*black*) and the trajectory with 2 mol% GWALP23 (*gray*).

the path length of the cell, c is the protein concentration, and N is the number of amino acids. The lipid background was subtracted from the experimental spectra.

Oriented circular dichroism

Dried lipid or peptide-lipid (peptide:lipid = 1:50 molar ratio) films were resuspended in methanol and deposited onto two circular quartz slides (Hellma Analytics, Müllheim, Germany). The solvent was evaporated by air flow for 3 h. The dried samples were rehydrated with 10 mM Na_3PO_4 (pH 7) for 15 h at room temperature at 96% relative humidity, obtained by using saturated K_2SO_4. The oriented circular dichroism (OCD) cell was sealed by the two quartz slides with the deposited samples and contained an inner cavity filled with saturated K_2SO_4 to humidify the sample throughout the experiment. To limit potential linear dichroism artifacts, the sample was rotated through 45° intervals, and the eight measurements were averaged for the final spectrum. Measurements were performed on a Jasco J-815 spectropolarimeter at room temperature. Similar to the circular dichroism (CD) measurements, the respective lipid blanks were subtracted, and raw data were converted into mean residue ellipticity. The theoretical transmembrane and peripheral peptide spectra were adapted from Wu et al. (37). The theoretical spectra were obtained for the fractional helicity of the peptide in each lipid-peptide condition, which was calculated from the CD data by comparing the values at 222 nm to the theoretical values of a complete α-helix and a random coil (38).

Electron paramagnetic resonance

Ld and Lo samples with 16PC or 7PC spin probes were prepared by rapid solvent exchange. Before measurement, samples were pelleted and transferred to 1.5–1.8 × 100-mm glass capillaries. Spectra were recorded on a Bruker (Billerica, MA) ELEXSYS E500 CW EPR Spectrometer operated at X-band frequency (9.4 GHz) with 0.8 Gauss modulation for the 16PC probe and 1.2 Gauss modulation for the 7PC probe. Spectra shown are the average of 20 scans obtained at 22°C.

RESULTS

We first measured the rigidity of the Ld phase and the Lo phase using single-phase GUVs for various lipid-only mixtures. Lipid mixtures in this study include: bSM/DOPC/chol, bSM/POPC/chol, DSPC/DOPC/chol, and DSPC/POPC/chol. Along a thermodynamic tieline, the fractions of Ld and Lo phases are described by the lever rule. By measuring the bending moduli of the tieline endpoint compositions, the rigidity of phases that would coexist can be compared. We used existing phase diagrams with high compositional resolution previously determined for the mixtures DSPC/DOPC/chol, DSPC/POPC/chol, bSM/POPC/chol, and bSM/DOPC/chol (7,11). With this set of mixtures, we can compare the bending energies of the pure Ld and Lo phases that would exhibit nanoscopic or macroscopic phase separation if they coexisted. Whereas mixtures in which the low-Tm lipid is entirely DOPC exhibit domains that are many microns in diameter, those with POPC have similar phase diagrams but with phase domains that are nanometers in diameter (6). We begin with endpoints of the lowest tieline of the Ld + Lo region. Lipid compositions examined in this work are shown in Fig. S1.

Coexisting Ld and Lo at the lower cholesterol tieline

The bending moduli of Lo phases were 2 to nearly 10 times greater than Ld phases, as shown in Table 1. The values for the Ld phases we examined range between 1.1 and 3.2×10^{-19} J. The bSM-containing Ld phases have greater bending moduli than the DSPC-containing Ld phases. For the Lo phases, we measured bending moduli from 6.4 to 10.2×10^{-19} J. For the four mixtures studied, the bSM-containing Lo phases have lower bending moduli than the DSPC-containing Lo phases.

These lipid-only mixtures provide a baseline for modeling the influence of transmembrane proteins. To model the plasma membrane with a significant protein component, we include the helical peptide GWALP23 in the lipid mixtures studied. We first examined whether the peptide changed the phase boundaries for nanoscopic and macroscopic systems by measuring FRET along a compositional trajectory. Sample compositions followed a line parallel to the lower tieline as depicted in Fig. 1 *A*. For the purpose of closely replicating all experimental conditions, compositional trajectories with and without peptide were prepared from the same lipid stocks (Fig. 1, *B–D*).

The trajectories with (*gray*) and without (*black*) GWALP23 for DSPC/DOPC/chol are shown in Fig. 1 *B*. FRET between DHE (donor, favors Lo) and FAST DiO (acceptor, favors Ld) is plotted with respect to DSPC fraction. For this system and this dye pair, both boundaries are clearly visible, marked by the shaded regions. Because the boundaries can be difficult to define for nanoscopic systems containing peptide, additional information is useful; thus, trajectories in Fig. 1, *C* and *D* correspond to the same trajectory in DSPC/POPC/chol but with an additional FRET pair. The boundary at the left-hand side is visible in FRET between Trp and DHE along the trajectory shown in Fig. 1 *C*. The lipid-only trajectory contains TOE rather than GWALP23. The shapes of the two curves differ markedly, which can be attributed to differences in the photophysics of energy transfer between the different probes and DHE. FRET between DHE and FAST DiO was simultaneously collected, shown in Fig. 1 *D*.

These data show that phase boundaries for both nanoscopic and macroscopic mixtures do not change within experimental uncertainty with addition of up to 2 mol%

TABLE 1 Bending Moduli of Ld and Lo Phases

	κ_{Ld} (10^{-19} J)	κ_{Lo} (10^{-19} J)
bSM/DOPC/chol	2.6 (0.4)	6.4 (0.3)
bSM/POPC/chol	3.2 (0.4)	6.7 (0.3)
DSPC/DOPC/chol	1.1 (0.2)	10.2 (0.5)
DSPC/POPC/chol	2.3 (0.3)	7.3 (0.4)

Ld bending moduli, κ_{Ld}, and Lo bending moduli, κ_{Lo}, for lower-tieline Ld and Lo of bSM/DOPC/chol, bSM/POPC/chol, DSPC/DOPC/chol, and DSPC/POPC/chol are given. Standard error in parentheses.

peptide. Therefore, peptide can be added to the same single-phase mixtures as the lipid-only mixtures to compare the Ld and Lo phases that would coexist.

To determine the fraction of peptide in each phase that would occur at equilibrium with coexisting Ld + Lo, and thus should be compared for rigidity measurements, we next investigated the partitioning of the peptide. As described above, partition coefficients can be determined by fitting FRET along the compositional trajectory to Eq. 2. The sample trajectory for DSPC/DOPC/chol parallel to the lower tieline as shown in Fig. 1 *A* and analogous trajectory for bSM/DOPC/chol were prepared with 1 mol% peptide. FRET between the GWALP23 tryptophan donor and DHE acceptor were fit to Eq. 2 to determine K_p. For both DSPC/DOPC/chol and bSM/DOPC/chol, the peptide partitioned favorably into the Ld phase (Fig. 2, *A* and *B*, respectively). The K_p of GWALP23 is 13 ± 2 in DSPC/DOPC/chol and 8 ± 1 in bSM/DOPC/chol. Thus, for lipid compositions along the lower tieline of the two-phase region, the Ld phase contains 13- or 8-fold more peptide than the Lo phase for DSPC and bSM mixtures, respectively.

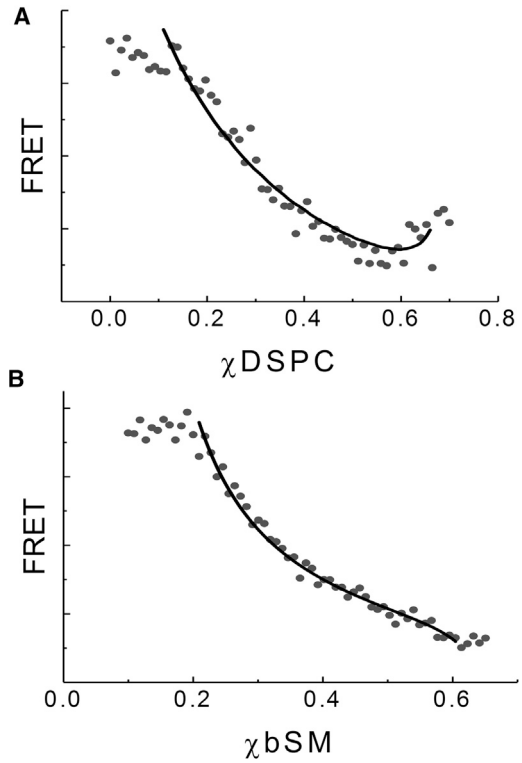

FIGURE 2 GWALP23 partitions favorably into the Ld phase. (*A*) FRET (*solid circles*, AU) from the GWALP23 tryptophan to DHE is plotted with respect to DSPC fraction along the trajectory for DSPC/DOPC/chol shown in Fig. 1 *A*. The best fit to Eq. 2 (*solid line*) yielded $K_p = 13 \pm 2$. (*B*) FRET (*solid circles*, AU) from the GWALP23 tryptophan to DHE is plotted with respect to bSM fraction along a trajectory parallel to the lower tieline of the two-phase region for bSM/DOPC/chol (11), with the best fit to Eq. 2 (*solid line*) yielding $K_p = 8 \pm 1$. Trajectories included 1 mol% GWALP23.

For DSPC/POPC/chol and bSM/POPC/chol, determining the K_p of GWALP23 between Ld and Lo is less straightforward because the domains are nanoscopic. Domains on DSPC/POPC/chol vesicles were previously measured to have a radius of 6.8 nm by small-angle neutron scattering (39). For bSM/POPC/chol, small-angle neutron scattering measurements suggest domains with radii less than 7 nm (11). Because domain size is near the magnitude of the Förster radius, R_0, the FRET efficiency is affected. Although Eq. 2 does not account for the size of domains, we estimated the GWALP23 partition coefficient in lipid mixtures that form nanodomains. To investigate K_p for these nanoscopic mixtures, we again studied sample trajectories parallel to the lower tieline. Trajectories using FRET from GWALP23 tryptophan to BODIPY-PC for DSPC/POPC/chol and for bSM/POPC/chol are shown in Fig. S2. Because both probes partition into the Ld phase, the shapes differ from those in Fig. 2. Without correcting for the small size of the domains, the best fit solid lines in Fig. S2 for the K_p of the peptide for DSPC/POPC/chol and bSM/POPC/chol is 4 ± 1 and 3 ± 1, respectively. The actual preference of the peptide for Ld would be larger than this fitting suggests because small domain size acts to reduce the influence on FRET of fluorophores separating or colocalizing.

With increasing peptide content, Ld bending moduli increase severalfold for all four mixtures examined (Fig. 3). The highest concentration of peptide that we could examine in GUVs was 4 mol%. Thus, the maximal peptide concentration that would be in the Lo phase would be 0.5 and 0.3 mol% for the coexisting lower tieline phases of bSM and DSPC mixtures given 8- and 13-fold preference for the Ld phase, respectively. This amount of peptide did not change the bending rigidity of the Lo phase (Fig. 3). The bending moduli of DSPC/DOPC/chol and DSPC/POPC/chol Ld phases increase with peptide, but the bending moduli are much less than those of the respective Lo phases. The bending moduli of bSM/DOPC/chol and bSM/POPC/chol Ld phases approach the bending moduli of the respective Lo phases with increasing peptide content. For bSM/POPC/chol, the rigidity of the Ld phase with transmembrane peptide exceeds that of the Lo phase.

We monitored the steady-state fluorescence of Trp and C12:0 DiI to evaluate the peptide incorporation in the final aqueous suspension of GUVs. In vesicles containing peptide, the intensity of the tryptophan fluorescence relative to the lipid concentration should be directly proportional to the peptide:lipid ratio. This ratio would be altered during sample preparation if the peptide fails to incorporate into the bilayer. We measured tryptophan fluorescence at ex/em = 280/330 nm in GUV samples like those used for the rigidity measurements but vortexed and diluted to reduce the contribution of light scattering. The observed tryptophan emission maximum of 330 nm is consistent with the peptide being in a hydrophobic environment for both Ld and Lo GUVs. Samples ranged from no peptide up to 4 mol% peptide. At the

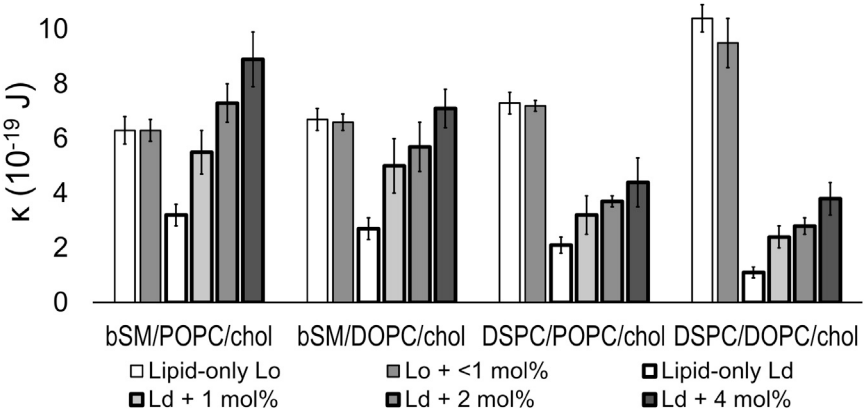

FIGURE 3 GWALP23 increases the membrane bending rigidity of the Ld phase. Bending moduli κ in 10^{-19} J for Ld (*bold outline*) and Lo (*light outline*), with GWALP23 (*shaded bars*) measured for bSM/POPC/chol, bSM/DOPC/chol, DSPC/POPC/chol, and DSPC/DOPC/chol.

amount included in our GUV samples, 0.1 mol%, C12:0 DiI fluorescence is directly proportional to the lipid concentration as determined by inorganic phosphate assay (32) (Fig. S3). The ratio of tryptophan fluorescence to C12:0 DiI fluorescence is plotted with respect to the mol% of peptide included in sample preparation in Fig. 4. The relationship is highly linear for Ld (Fig. 4 *A*), and thus the peptide:lipid ratio in Ld samples does not deviate from expected values. In contrast, the peptide:lipid ratio decreases for Lo phase samples with greater than 1 mol% GWALP23 (Fig. 4 *B*). The deviation from linearity for the 2 and 4 mol% Lo samples implies that the peptide is depleted during sample preparation. Thus, we limited our bending moduli observations for Lo phase to 1 mol% peptide or less.

We examined the structure and orientation of the peptide with CD and OCD. WALP-like peptides typically acquire helical structure when embedded in lipid membranes (40,41). We observed clearly helical features in the CD spectrum of the GWALP23 peptide in the Ld phase, with minima at 222 and 208 nm and a maximum at 195 nm (42) (Fig. 5 *A*). However, the CD spectrum obtained in Lo lipids was strikingly different. Although the same helical features were observed, the spectrum showed a large intensity decrease. The helicity of GWALP23 in Ld and Lo was estimated to be 56 and 7%, respectively (38). Although the former value is expected for a transmembrane peptide and is consistent with solid-state ^{2}H NMR measurements for GWALP23 (28), the latter value was too low to be compatible with a transmembrane peptide. Consistent with the results in Fig. 4 *B*, the CD in Lo lipids implies that at 2 mol %, GWALP23 is not efficiently incorporating into the Lo phase of these extruded vesicles.

We then performed OCD experiments in hydrated supported bilayers, which inform on the orientation of helical structures with respect to the bilayer. The OCD spectrum of GWALP23 in Ld bilayers overlapped with the corresponding theoretical transmembrane curve, demonstrating that the peptide indeed adopted a transmembrane orientation in Ld. However, the spectrum of GWALP23 in Lo bilayers indicated that the peptide no longer adopted a transmembrane state. In fact, the OCD spectrum in Lo lipids was closer to the theoretical curve corresponding to a helix on the membrane surface, implying that in these conditions GWALP23 was a surface-bound helix. Thus, the OCD spectra revealed that the insertion propensity of GWALP23 shifted from an inserted α-helix configuration in Ld lipids (Fig. 5 *B*) toward a noninserted one in Lo lipids (Fig. 5 *C*). Figure 4 implies that the peptide:lipid ratio is

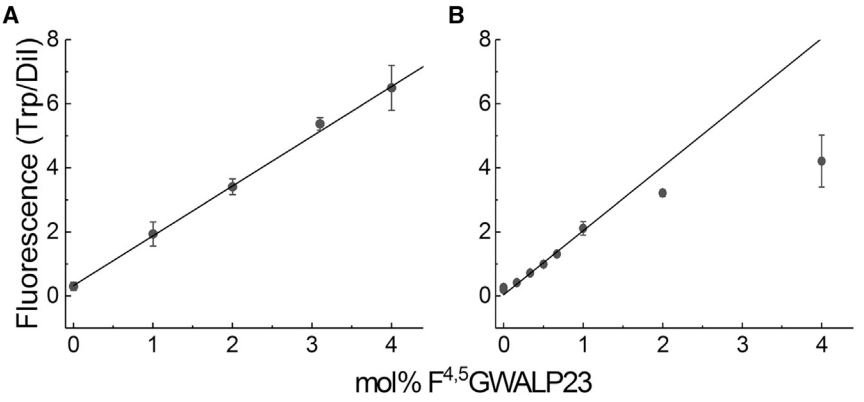

FIGURE 4 The ratio of GWALP23:lipid does not change during GUV preparation for DSPC/DOPC/chol Ld up to 4 mol% GWALP23, and for Lo up to 1 mol% GWALP23 in Lo. (*A*) The ratio of Trp to C12:0 DiI fluorescence in DSPC/DOPC/chol Ld is shown. (*B*) The ratio of Trp to C12:0 DiI fluorescence in DSPC/DOPC/chol Lo.

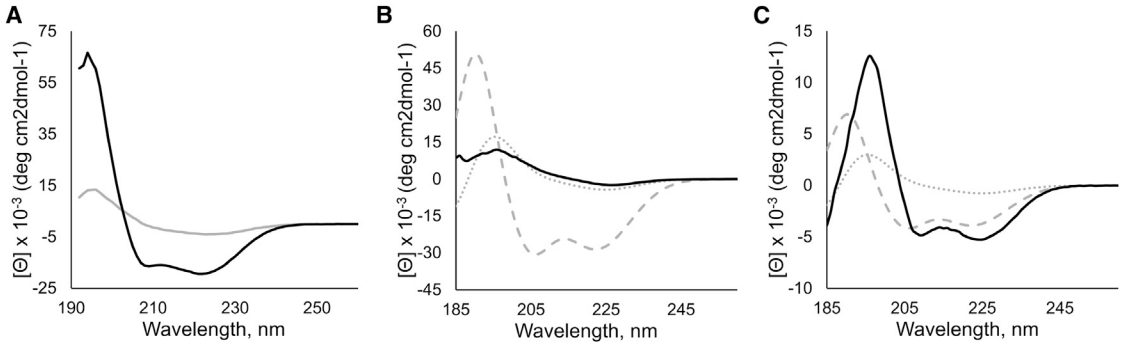

FIGURE 5 Structure and orientation of GWALP23 in DSPC/DOPC/chol Ld and Lo. (*A*) CD spectra of GWALP23 in Ld phase (*black*) and Lo phase (*gray*) are shown. (*B* and *C*) OCD spectra of GWALP23 in hydrated stacked Ld (*B*) and Lo (*C*) lipid bilayers are shown. The dotted and dashed lines correspond to theoretical OCD spectra for an ideal α-helix aligned parallel (*dotted*) and perpendicular (*dashed*) to the membrane normal; the spectra correspond to transmembrane and peripheral helical peptides, respectively. The significant difference in helicity (7% versus 56%) resulted in the variation in the theoretical curves for GWALP23 in Ld (*B*) and Lo (*C*).

as expected up to 1 mol%. From the characteristic shape of the FRET curves for partition coefficient determination with 0.5 mol% (Figs. 2 and S2), we conclude that the peptide is participating in FRET with the cholesterol analog, DHE, implying insertion. Higher concentrations seem to exceed the capacity of the Lo phase for peptide, based on the OCD data at 2 mol% and Fig. 4 *B*.

In an effort to understand how the peptide affects the Ld and Lo phases, we conducted electron paramagnetic resonance (EPR) experiments using 7PC and 16PC probes, wherein the paramagnetic labels are located near the middle or end of the hydrocarbon chain, respectively. We measured the order parameter at these positions of the acyl chains in DSPC/DOPC/chol. Changes in the phases caused by the peptide could inform our interpretation of bending modulus measurements and insertion. We found that the peptide does not affect order of Ld lipids; see Fig. S4 and Table S3. This finding implies that the peptide changes the Ld bending modulus without changing the local ordering in the phase. Though this differs from biologically unusual, but well-studied, peptides like gramicidin (43), it is consistent with unchanged phase boundaries and previous studies of WALP peptides in bilayers without cholesterol (44).

High-cholesterol tieline Ld and Lo

From existing phase diagrams, the lowest tieline endpoint compositions correspond to the coexisting Ld and Lo phases that differ the most in composition. As cholesterol content increases, tieline length decreases, becoming zero at the critical point where Ld and Lo do not differ compositionally and spontaneously interconvert. To compare the bending rigidity of the more similar Ld and Lo phases, we examined tieline endpoints at higher cholesterol content. Assuming the tielines fan out evenly between the slope of the lower boundary and the slope of the tangent line at the critical point (45), we interpolated between the slope of the lower boundary of the two-phase region and the slope of the line tangent to the boundary at the putative critical point. The compositions chosen are shown in Fig. S1. Near the critical points for each of the four mixtures, the bending moduli of Ld and Lo are closer in magnitude than the lower tieline compositions (Table 2).

We investigated the effects of the peptide on phase behavior and membrane bending moduli of the more compositionally similar Ld and Lo phases of DSPC/DOPC/chol at higher cholesterol fractions. We continued our investigations with DSPC/DOPC/chol because we have a greater confidence in the critical point location determined for this mixture in previous work (7), and, as a result, the appropriate tieline slope to use for higher tieline measurements. We again used FRET trajectories to define phase boundaries and to determine the K_p of the peptide at these higher cholesterol fractions. The slope of the high-cholesterol trajectory was determined as described above. We found the phase boundaries were unchanged by the presence of 1 mol% peptide (Fig. 6). The K_p of the peptide was found to be 3 ± 1 favoring the Ld phase (Fig. 7). The K_p of DHE approaches 1 at this higher cholesterol tieline, and, for that reason, the shape of the FRET curve in Fig. 7 differs markedly from those in Fig. 2. Consistent with this decrease of DHE K_p as cholesterol fraction increases, a decrease in K_p of ~3-fold from the lower to the higher tieline in the two-phase region was also observed for FAST DiO (Fig. S5).

TABLE 2 Bending Moduli of High-Cholesterol Ld and Lo Phases

	κ_{Ld} (10^{-19} J)	κ_{Lo} (10^{-19} J)
bSM/DOPC/chol	2.5 (0.4)	3.1 (0.3)
bSM/POPC/chol	2.7 (0.2)	3.1 (0.2)
DSPC/DOPC/chol	2.4 (0.4)	2.8 (0.3)
DSPC/POPC/chol	2.3 (0.1)	3.1 (0.3)

Ld bending moduli, κ_{Ld}, and Lo bending moduli, κ_{Lo}, for high-cholesterol Ld and Lo of bSM/DOPC/chol, bSM/POPC/chol, DSPC/DOPC/chol, and DSPC/POPC/chol are given. Standard error in parentheses.

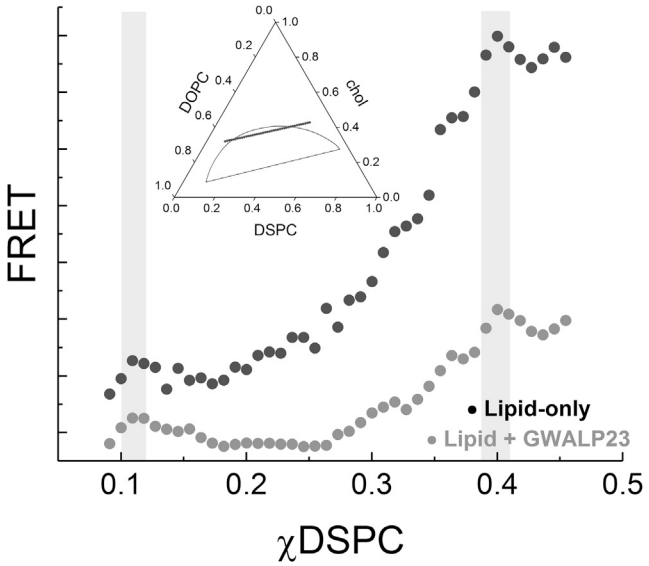

FIGURE 6 The presence of 2 mol% GWALP23 does not change phase boundaries of DSPC/DOPC/chol at high cholesterol fraction. FRET from DHE to FAST DiO is shown along the trajectory in the inset in the absence (*black*, *upper*) and in the presence of 1 mol% GWALP23 (*gray*, shifted lower for clarity). Boundaries correspond to the shaded regions. The width of each shaded region is the fitting error.

Given the smaller K_p of the peptide between Ld and Lo phases at high-cholesterol fraction, we compared the Ld phase with increasing concentrations of peptide to the Lo phase with no peptide and with 1 mol% GWALP23 in Fig. 8. The peptide increases the bending modulus of the Ld phase, and at 2 mol% peptide, the bending modulus of the Ld phase is greater than that of the Lo phase with 1 mol% peptide.

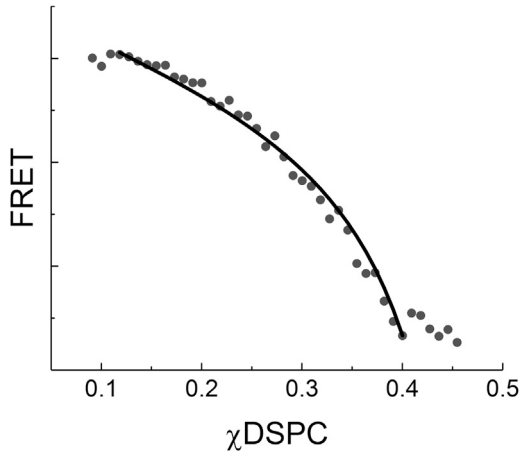

FIGURE 7 GWALP23 partitions into the Ld phase at high cholesterol fraction. FRET from the GWALP23 tryptophan to DHE is plotted with respect to DSPC fraction along the trajectory for DSPC/DOPC/chol shown in Fig. 6, inset, with 1 mol% GWALP23. The best fit (*solid line*) to Eq. 2 yields $K_p = 3 \pm 1$.

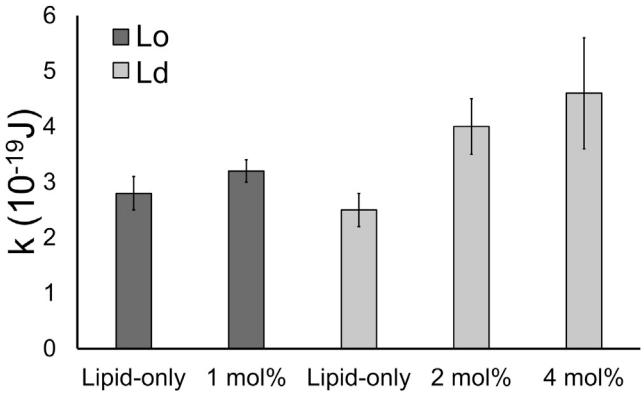

FIGURE 8 GWALP23 increases the rigidity of the Ld phase at the high cholesterol tieline for DSPC/DOPC/chol. Bending moduli κ of Ld (*light bars*) and Lo (*dark bars*) at these higher tieline endpoint compositions were measured. The bending modulus is shown for the Ld phase with 2 and 4 mol% GWALP23. Error bars reflect standard error.

Difference in Ld and Lo bending moduli of various models

As we have shown, the membrane bending moduli of Ld and Lo become very similar at higher cholesterol fractions. A separate issue is how well commonly used, simplified mixtures model the behavior of coexisting phases. We simplify the mixtures by using a pure low-Tm lipid (DOPC or POPC) for Ld and a binary high-Tm lipid/chol for Lo. In Fig. 9, simplified, lower-tieline, and high-cholesterol Ld and Lo compositions are shown by the line endpoints on the representative diagram. Simplified mixtures are at extremes of the diagram, coinciding with the low-Tm vertex for Ld and the high-Tm/chol binary axis for Lo. The lower-tieline compositions are shown at the bottom of the two-phase region, and high-cholesterol compositions are near the top. Compositions were chosen based on published phase diagrams for each mixture (5,6) and are plotted in Fig. S1. The difference in bending moduli, $\Delta\kappa = \kappa_{Lo} - \kappa_{Ld}$, for each set of simple, lower-tieline, and high-cholesterol for bSM/POPC/chol, bSM/DOPC/chol, DSPC/POPC/chol, and DSPC/DOPC/chol, is plotted with respect to distance in compositional space. This distance is calculated as a three-dimensional Euclidean distance normalized to one side of the ternary diagram. Thus, the simplified mixtures are the furthest apart in both composition and in bending moduli, and the high-cholesterol tieline endpoints are the closest. For comparison to the ternary mixtures, we measured the bending moduli of a simplified Ld phase, DOPC, with peptide. We found the bending modulus increased with peptide concentration, and this increase was more gradual than in the ternary Ld compositions (Fig. S6).

DISCUSSION

Many cellular functions and structures require membrane deformation, subjecting the membrane to mechanical stress.

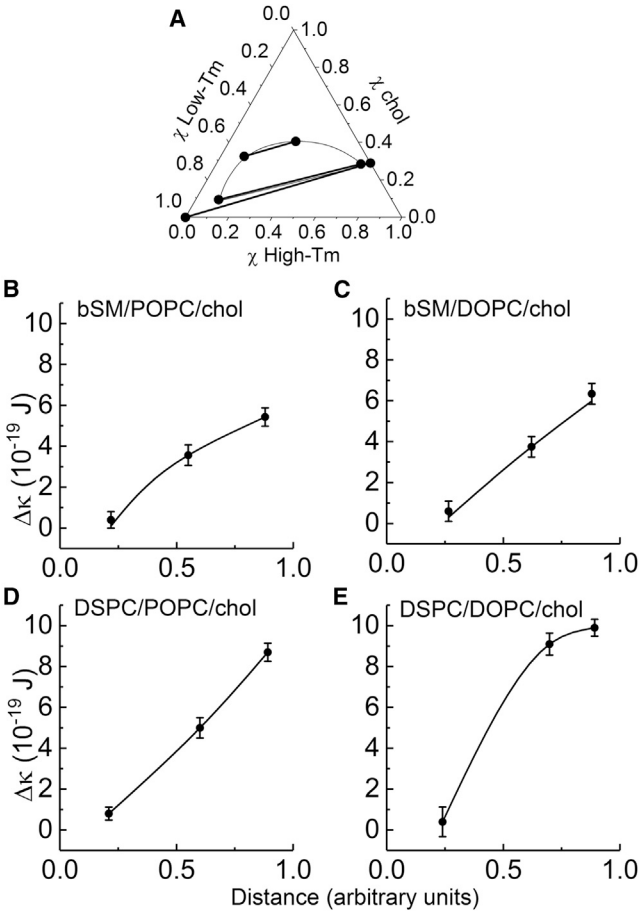

FIGURE 9 Bending moduli of Ld and Lo phases in lipid-only mixtures. (*A*) The compositions we compared are shown representatively as line endpoints on the generic phase diagram above. Simplified, lower-tieline, and high-cholesterol Ld and Lo compositions for bSM/POPC/chol, bSM/DOPC/chol, DSPC/POPC/chol, and DSPC/DOPC/chol are plotted in Fig. S1. The difference in bending moduli, $\Delta\kappa = \kappa_{Lo} - \kappa_{Ld}$, between simple, lower-tieline, and high-cholesterol Lo and Ld phases for bSM/POPC/chol (*A*), bSM/DOPC/chol (*B*), DSPC/POPC/chol (*C*), and DSPC/DOPC/chol (*D*) is plotted with respect to distance in composition space or the compositional separation of Ld and Lo phases.

As expected, others have found raft-like Lo phases to have membrane bending moduli greater than those of Ld for both single phases (2,13,14) and coexisting phases (15). These results, together with a correlation between raft-like composition and curvature, raise questions about what the rigidity difference is between phases in models that more closely resemble the plasma membrane and how the components of the membrane affect rigidity. Membrane bending moduli decrease with increasing degree of *cis* unsaturation (46) and increase with hydrophobic thickness of the membrane (46,47). Cholesterol has been found to rigidify membranes composed of low-Tm lipids in which at least one chain is saturated but not membranes in which both chains are unsaturated, such as DOPC (13,14,48,49). The mixtures used in this study offer a range of physiological relevance. bSM as the high-Tm lipid is more representative than DSPC, POPC is naturally more abundant than DOPC in animal cell plasma membranes, and the higher-cholesterol content we examined is physiologically more relevant than that of the lower-tieline endpoints (50–52). For each mixture, we have focused on Ld and Lo phases that would coexist, and we sought to address the effects of a peptide component in the context of these phases.

Coexisting Ld and Lo at the lower-cholesterol tieline

The bending moduli of lower-tieline Lo phases are much greater than those of the corresponding Ld phases (Table 1). Others have also suggested or measured the bending rigidity of the Lo phase to be several times greater than that of the Ld phase (53–55). With ternary mixtures, the accuracy of the measurement is limited somewhat by the variation between vesicles. Our measurement of the DSPC/DOPC/chol Ld phase is consistent with measurements by other groups and other methods (54), and in only this case, near to measurements for one-component membranes of the major component, DOPC (13,56). When overall composition is similar, the mixtures containing POPC have greater membrane bending moduli than those containing DOPC, consistent with the findings of others (14). The presence of cholesterol likely increases this rigidity difference because POPC has a saturated acyl chain and DOPC does not (49,57). For the Ld compositions in Table 1, it can be seen that DOPC mixtures are less rigid than the corresponding mixtures with POPC. This trend does not hold for the DSPC Lo compositions because of the difference in phase boundaries between DSPC/DOPC/chol and DSPC/POPC/chol. The DSPC/POPC/chol Lo phase has 15 mol% low-melting lipid, whereas the corresponding DOPC mixture has only 3 mol%.

Comparing the DSPC mixtures to the bSM mixtures at the lowest tieline, the length of the tieline for bSM mixtures is shorter than that of the DSPC mixtures, meaning that the bSM Ld and Lo phases are compositionally more similar. In contrast to the respective DSPC Lo phases with a fivefold difference in the amount of low-Tm lipid, the difference in the amount of low-Tm lipid is less than twofold, with 7 mol% low-Tm lipid in the bSM/POPC/chol Lo phase and 4 mol% in the bSM/DOPC/chol Lo phase. This similarity in the overall Lo composition for bSM/DOPC/chol and bSM/POPC/chol results in similar bending moduli. For the Ld phases, although the DSPC-containing Ld phases have 80% low-Tm lipid (Fig. S1), bSM/DOPC/chol and bSM/POPC/chol contain only 70 mol% low-Tm lipid, consistent with their higher bending moduli (Table 1).

The GWALP peptide used in this study partitions favorably into the Ld phase. In the mixtures for which we can conclusively determine the K_p as described, the peptide concentration is ~10-fold greater in the Ld phase when Ld and Lo coexist in these mixtures. Preference for Ld phase is

usual for transmembrane proteins (58). Though commonly considered "raftophilic," GPI-anchored proteins are, at best, not excluded from the more ordered phase (59,60). In giant plasma membrane vesicles, inclusion of transmembrane helices in the more ordered phase is dependent on palmitoylation, and even palmitoylated peptides still have a K_p near 1, i.e., they do not strongly favor the more ordered phase (61).

We find that GWALP23 peptide increases the rigidity of the Ld phase. With increasing peptide content, the bending moduli of the Ld phase approaches that of the Lo phase, and in the case of the bSM/POPC/chol mixture with 4 mol% peptide, the rigidity of the Ld phase exceeds that of the Lo phase. The increases in the Ld bending moduli with 4 mol% peptide compared to the lipid-only Ld were 2.8-, 2.6-, 2.1-, and 3.4-fold for bSM/POPC/chol, bSM/DOPC/chol, DSPC/POPC/chol, and DSPC/DOPC/chol, respectively. With peptide included in an amount consistent with the K_p and below 1 mol%, the Lo bending moduli are unchanged.

GWALP23 incorporation and orientation in the bilayer

Whereas proteins make up about half of the total mass of the plasma membrane, the volume of the bilayer interior that is protein is closer to 20% (2,3). A similar volume fraction of transmembrane peptide in our vesicle preparations would be ~9 mol% GWALP23 (62,63). We could not prepare GUVs with such a high fraction of peptide. The highest concentration of peptide that we could examine in Ld GUVs was 4 mol%. Perhaps the increased membrane rigidity inhibits the spontaneous formation of GUVs. Consistent with this possibility, we could prepare GUVs of DOPC, which are less rigid than those having the ternary compositions, with up to 6 mol% peptide (Fig. S6).

In our investigations of GWALP23 structure using CD, we found low signal amplitude for the peptide in Lo. The OCD measurements to examine the orientation of the peptide revealed that although the peptide was inserted with a low tilt angle from the bilayer normal in the Ld phase, this was not the case for the Lo phase. In Ld, the extent of helix and the helix tilt are consistent with NMR measurements in single-component bilayers (28). In Lo, the OCD spectrum is consistent with the peptide being oriented perpendicular to the membrane normal. Given the shift away from inserted to surface-bound for oriented Lo bilayers with 2 mol% peptide, the loss of peptide after extrusion of the vesicles to form 100-nm LUVs is likely due to GWALP23 not being inserted. As the theoretical OCD curves depend on the percentage of helical residues, the significant difference in helicity resulted in the variation in the theoretical curves for GWALP23 in Lo (Fig. 5 *B*) and Ld (Fig. 5 *C*).

Our observations with OCD are consistent with the findings in Fig. 4. The peptide:lipid ratio appears to be as anticipated up to 4 mol% in Ld, but this is not the case with Lo GUV preparations. The apparent peptide:lipid ratio in Lo begins to deviate from expected values with greater than 1 mol% (Fig. 4). FRET curves that we could fit to a partition coefficient required 1 mol% GWALP23 or less. FRET measurements between GWALP23 Trp and membrane-bound DHE or BODIPY-PC reveal a characteristic shape that can only occur if the peptide is located within the bilayer of these nonextruded vesicles. We conclude the peptide is inserted at this low concentration. Because GWALP23 partitions ~3- to 10-fold favoring the Ld phase, we compare the bending energy of an Ld phase containing peptide with an Lo phase containing ~3- to 10-fold-less peptide. Given the peptide concentrations for which we could obtain Ld GUVs and our conclusions regarding incorporation in the Lo phase, our Lo phases for the bending moduli measurements contain less than 1 mol% GWALP23.

High-cholesterol tieline Ld and Lo

The more compositionally similar Ld and Lo phases at higher cholesterol fractions are more physiologically relevant, given the typical cholesterol content of 40–50 mol% in the animal cell membrane (52). The difference in bending moduli between Ld and Lo at higher cholesterol content becomes small for all of the lipid-only cases. The difference in bending moduli at the high-cholesterol compositions is greatest for DSPC/POPC/chol. Because of the shape of the two-phase region for this mixture, the compositions chosen for comparison at a higher tieline are farther apart in compositional space. Further, these DSPC/POPC/chol compositions nearer to the critical point did not contain as much cholesterol as the other high-cholesterol compositions (Fig. S1).

The phase boundaries for the high-cholesterol compositions of DSPC/DOPC/chol with up to 1 mol% GWALP23 did not differ from the phase boundaries without peptide, as observed for the low-cholesterol compositions. The peptide still favors the Ld phase, although the K_p of 3 at high cholesterol is ~4-fold lower than the K_p of 13 at low cholesterol. A similar change in K_p was also observed for FAST DiO. This is, perhaps, not surprising, given the greater similarity of the Ld and Lo compositions.

The transmembrane peptide increased the rigidity of the DSPC/DOPC/chol Ld phase at high-cholesterol fraction. The bending modulus of Ld with 4 mol% peptide is twofold greater than that of the lipid-only Ld phase and 1.4-fold greater than that of the Lo phase. Further, using the measured peptide K_p of 3, the Ld phase with 4 mol% GWALP23 becomes more rigid than the Lo phase with 1 mol% GWALP23, for which the respective fractions of peptide are representative of distribution between Ld and Lo when they coexist. At near-physiological cholesterol content and with a significant fraction of the membrane volume being occupied by transmembrane helices, the bending

modulus of the disordered phase is greater than that of the ordered phase.

Increased membrane bending rigidity with GWALP23

Both simulation and experimental data have indicated that WALP peptides could alter bilayer thickness (44,64). Deviations from the equilibrium bilayer thickness would undoubtedly contribute to increased membrane bending rigidity. However, the changes in bilayer thickness observed experimentally are slight and likely do not account for the entirety of the increase in bending moduli of Ld phases with GWALP23.

GWALP23 has been shown experimentally and in molecular dynamics simulations to change the size of domains (34,64). Molecular dynamics simulations of the peptide in membrane compositions mimicking those used here suggest that the peptide increases domain registration and is depleted from the domain interface (64). Both the increase in domain size and the interface depletion imply increased line tension. However, as the EPR data show (Fig. S4 and Table S3), these changes are not accomplished through changes in ordering in the phase. Increased domain registration in the two leaflets, as observed in simulations in the presence of peptide, could point to a mechanism for increased rigidity of the Ld phase.

By spanning the bilayer, the peptide could reduce the ability of the leaflets to slide relative to each other. Rather than the bilayer consisting of two elastic sheets fluctuating somewhat independently, a bilayer with fully coupled leaflets is effectively one elastic sheet of double the thickness with a bending modulus greater than the uncoupled bilayer (14,65). The bending moduli of the four different Ld phases showed increases ranging from 2- to 3.5-fold with 4 mol% GWALP23.

Simplified mixtures are not representative of coexisting phases

The measurements discussed above were for the lower- and high-cholesterol tielines of the two-phase region. We also compared these ternary Ld and Lo compositions to commonly used single-component or binary mixtures. From Fig. 9, we see that the simplified phases are only representative in the case of the DSPC/DOPC/chol lower-cholesterol compositions. The bending moduli of the ternary Ld and Lo phases of bSM/DOPC/chol and bSM/POPC/chol differed significantly from the simplified models. The Ld phases had bending moduli up to three times greater than the simple Ld phases, and the actual Lo phases in the Ld + Lo coexistence region had bending moduli ~10% smaller than the simple Lo phase outside this region. Thus, these simplified models are perhaps less representative of the more physiological Ld or Lo phases that would coexist.

CONCLUSIONS

In this work, we begin to address how a transmembrane α-helical peptide influences bilayer mechanical properties. GWALP23 exhibits a preference for the Ld phase but does not change phase boundaries. We determined the rigidity of the Ld and Lo phases that coexist by independently measuring the rigidity of single-phase GUVs of the compositions at the tieline endpoints. GWALP23 transmembrane peptide causes a striking increase in the bending modulus of the Ld phase for all mixtures in this study. We examined the effects of the peptide at high, more physiological cholesterol content and found that the peptide causes the bending modulus of the Ld phase to surpass that of the Lo phase. We compared the rigidity of these lipid-only lower-tieline compositions to the rigidity of the Ld + Lo phases coexisting at higher-cholesterol content and to simplified Ld and Lo compositions. We found that the ternary mixtures differed significantly from the simplified phases, and the difference in Ld and Lo rigidity decreases at high-cholesterol content.

SUPPORTING MATERIAL

Supporting Materials and Methods, six figures, and three tables are available at http://www.biophysj.org/biophysj/supplemental/S0006-3495(18)30395-3.

AUTHOR CONTRIBUTIONS

R.D.U. designed and performed the research, analyzed the data, and wrote the article. T.A.E., S.P.W., V.P.N., and F.N.B. designed and performed the research, analyzed the data, and contributed in writing the article. D.G.A. designed experiments. R.E.K. and D.V.G. designed, synthesized, and purified $F^{4,5}$GWALP23 and contributed peptide expertise. G.W.F. designed the research, analyzed the data, and cowrote the article.

ACKNOWLEDGMENTS

We thank Paulo Almeida, Chung-Yuen Hui, and Stuart Phoenix for helpful discussions.

This work was supported by U.S. National Science Foundation grant No. MCB-1410926 and U.S. National Institutes of Health (NIH) grant No. GM105684 (to G.W.F.); NIH grant No. GM120642 (to F.N.B); NIH Training grant No. 1-T32-GM08267 (to D.G.A.); National Science Foundation Graduate Research Fellowship Program under grant No. DGE-1144153ESR (to R.D.U.); Brazil Conselho Nacional de Desenvolvimento Científico e Tecnológico, CNPq (to T.A.E.); and National Science Foundation grants MCB-1327611 and -1713242 to R.E.K. and D.V.G. EPR studies were supported by NIH/National Institute of General Medical Sciences grant No. P41GM103521 to J. Freed.

REFERENCES

1. McMahon, H. T., and J. L. Gallop. 2005. Membrane curvature and mechanisms of dynamic cell membrane remodelling. *Nature*. 438:590–596.
2. Roux, A., D. Cuvelier, …, B. Goud. 2005. Role of curvature and phase transition in lipid sorting and fission of membrane tubules. *EMBO J.* 24:1537–1545.

3. Aimon, S., A. Callan-Jones, …, P. Bassereau. 2014. Membrane shape modulates transmembrane protein distribution. *Dev. Cell.* 28:212–218.
4. Feigenson, G. W., and J. T. Buboltz. 2001. Ternary phase diagram of dipalmitoyl-PC/dilauroyl-PC/cholesterol: nanoscopic domain formation driven by cholesterol. *Biophys. J.* 80:2775–2788.
5. Zhao, J., J. Wu, …, G. W. Feigenson. 2007. Phase studies of model biomembranes: complex behavior of DSPC/DOPC/cholesterol. *Biochim. Biophys. Acta.* 1768:2764–2776.
6. Heberle, F. A., J. Wu, …, G. W. Feigenson. 2010. Comparison of three ternary lipid bilayer mixtures: FRET and ESR reveal nanodomains. *Biophys. J.* 99:3309–3318.
7. Konyakhina, T. M., J. Wu, …, G. W. Feigenson. 2013. Phase diagram of a 4-component lipid mixture: DSPC/DOPC/POPC/chol. *Biochim. Biophys. Acta.* 1828:2204–2214.
8. Marsh, D. 2009. Cholesterol-induced fluid membrane domains: a compendium of lipid-raft ternary phase diagrams. *Biochim. Biophys. Acta.* 1788:2114–2123.
9. Veatch, S. L., K. Gawrisch, and S. L. Keller. 2006. Closed-loop miscibility gap and quantitative tie-lines in ternary membranes containing diphytanoyl PC. *Biophys. J.* 90:4428–4436.
10. Uppamoochikkal, P., S. Tristram-Nagle, and J. F. Nagle. 2010. Orientation of tie-lines in the phase diagram of DOPC/DPPC/cholesterol model biomembranes. *Langmuir.* 26:17363–17368.
11. Petruzielo, R. S., F. A. Heberle, …, G. W. Feigenson. 2013. Phase behavior and domain size in sphingomyelin-containing lipid bilayers. *Biochim. Biophys. Acta.* 1828:1302–1313.
12. Bezlyepkina, N., R. S. Gracià, …, R. Dimova. 2013. Phase diagram and tie-line determination for the ternary mixture DOPC/eSM/cholesterol. *Biophys. J.* 104:1456–1464.
13. Gracià, R. S., N. Bezlyepkina, …, R. Dimova. 2010. Effect of cholesterol on the rigidity of saturated and unsaturated membranes: fluctuation and electrodeformation analysis of giant vesicles. *Soft Matter.* 6:1472–1482.
14. Marsh, D. 2006. Elastic curvature constants of lipid monolayers and bilayers. *Chem. Phys. Lipids.* 144:146–159.
15. Baumgart, T., S. Das, …, J. T. Jenkins. 2005. Membrane elasticity in giant vesicles with fluid phase coexistence. *Biophys. J.* 89:1067–1080.
16. Simons, K., and G. van Meer. 1988. Lipid sorting in epithelial cells. *Biochemistry.* 27:6197–6202.
17. Brügger, B., B. Glass, …, H. G. Kräusslich. 2006. The HIV lipidome: a raft with an unusual composition. *Proc. Natl. Acad. Sci. USA.* 103:2641–2646.
18. Takamori, S., M. Holt, …, R. Jahn. 2006. Molecular anatomy of a trafficking organelle. *Cell.* 127:831–846.
19. Hering, H., C. C. Lin, and M. Sheng. 2003. Lipid rafts in the maintenance of synapses, dendritic spines, and surface AMPA receptor stability. *J. Neurosci.* 23:3262–3271.
20. Dinic, J., P. Ashrafzadeh, and I. Parmryd. 2013. Actin filaments attachment at the plasma membrane in live cells cause the formation of ordered lipid domains. *Biochim. Biophys. Acta.* 1828:1102–1111.
21. Beloribi-Djefaflia, S., S. Vasseur, and F. Guillaumond. 2016. Lipid metabolic reprogramming in cancer cells. *Oncogenesis.* 5:e189.
22. Cross, S. E., Y. S. Jin, …, J. K. Gimzewski. 2007. Nanomechanical analysis of cells from cancer patients. *Nat. Nanotechnol.* 2:780–783.
23. Killian, J. A., I. Salemink, …, D. V. Greathouse. 1996. Induction of nonbilayer structures in diacylphosphatidylcholine model membranes by transmembrane α-helical peptides: importance of hydrophobic mismatch and proposed role of tryptophans. *Biochemistry.* 35:1037–1045.
24. Vostrikov, V. V., A. E. Daily, …, R. E. Koeppe, II. 2010. Charged or aromatic anchor residue dependence of transmembrane peptide tilt. *J. Biol. Chem.* 285:31723–31730.
25. Andersen, O. S., and R. E. Koeppe, II. 2007. Bilayer thickness and membrane protein function: an energetic perspective. *Annu. Rev. Biophys. Biomol. Struct.* 36:107–130.
26. Gleason, N. J., V. V. Vostrikov, …, R. E. Koeppe, II. 2012. Tyrosine replacing tryptophan as an anchor in GWALP peptides. *Biochemistry.* 51:2044–2053.
27. Sparks, K. A., N. J. Gleason, …, R. E. Koeppe, II. 2014. Comparisons of interfacial Phe, Tyr, and Trp residues as determinants of orientation and dynamics for GWALP transmembrane peptides. *Biochemistry.* 53:3637–3645.
28. Mortazavi, A., V. Rajagopalan, …, R. E. Koeppe, II. 2016. Juxta-terminal helix unwinding as a stabilizing factor to modulate the dynamics of transmembrane helices. *ChemBioChem.* 17:462–465.
29. Almén, M. S., K. J. Nordström, …, H. B. Schiöth. 2009. Mapping the human membrane proteome: a majority of the human membrane proteins can be classified according to function and evolutionary origin. *BMC Biol.* 7:50.
30. Krogh, A., B. Larsson, …, E. L. Sonnhammer. 2001. Predicting transmembrane protein topology with a hidden Markov model: application to complete genomes. *J. Mol. Biol.* 305:567–580.
31. Sharpe, H. J., T. J. Stevens, and S. Munro. 2010. A comprehensive comparison of transmembrane domains reveals organelle-specific properties. *Cell.* 142:158–169.
32. Kingsley, P. B., and G. W. Feigenson. 1979. The synthesis of a perdeuterated phospholipid: 1,2-dimyristoyl-sn-glycero-3-phosphocholine-d72. *Chem. Phys. Lipids.* 24:135–147.
33. Akashi, K., H. Miyata, …, K. Kinosita, Jr. 1996. Preparation of giant liposomes in physiological conditions and their characterization under an optical microscope. *Biophys. J.* 71:3242–3250.
34. Usery, R. D., T. A. Enoki, …, G. W. Feigenson. 2017. Line tension controls liquid-disordered + liquid-ordered domain size transition in lipid bilayers. *Biophys. J.* 112:1431–1443.
35. Buboltz, J. T., and G. W. Feigenson. 1999. A novel strategy for the preparation of liposomes: rapid solvent exchange. *Biochim. Biophys. Acta.* 1417:232–245.
36. Buboltz, J. T. 2007. Steady-state probe-partitioning fluorescence resonance energy transfer: a simple and robust tool for the study of membrane phase behavior. *Phys. Rev. E Stat. Nonlin. Soft Matter Phys.* 76:021903–021907.
37. Wu, Y., H. W. Huang, and G. A. Olah. 1990. Method of oriented circular dichroism. *Biophys. J.* 57:797–806.
38. Ladokhin, A. S., M. Fernández-Vidal, and S. H. White. 2010. CD spectroscopy of peptides and proteins bound to large unilamellar vesicles. *J. Membr. Biol.* 236:247–253.
39. Heberle, F. A., R. S. Petruzielo, …, J. Katsaras. 2013. Bilayer thickness mismatch controls domain size in model membranes. *J. Am. Chem. Soc.* 135:6853–6859.
40. Thomas, R., V. V. Vostrikov, …, R. E. Koeppe, II. 2009. Influence of proline upon the folding and geometry of the WALP19 transmembrane peptide. *Biochemistry.* 48:11883–11891.
41. Killian, J. A. 2003. Synthetic peptides as models for intrinsic membrane proteins. *FEBS Lett.* 555:134–138.
42. Kelly, S. M., T. J. Jess, and N. C. Price. 2005. How to study proteins by circular dichroism. *Biochim. Biophys. Acta.* 1751:119–139.
43. Beaven, A. H., A. J. Sodt, …, W. Im. 2017. Characterizing residue-bilayer interactions using gramicidin A as a scaffold and tryptophan substitutions as probes. *J. Chem. Theory Comput.* 13:5054–5064.
44. de Planque, M. R., D. V. Greathouse, …, J. A. Killian. 1998. Influence of lipid/peptide hydrophobic mismatch on the thickness of diacylphosphatidylcholine bilayers. A 2H NMR and ESR study using designed transmembrane α-helical peptides and gramicidin A. *Biochemistry.* 37:9333–9345.
45. Francis, A. W. 1963. Liquid-liquid Equilibriums. Interscience Publishers, New York.
46. Rawicz, W., K. C. Olbrich, …, E. Evans. 2000. Effect of chain length and unsaturation on elasticity of lipid bilayers. *Biophys. J.* 79:328–339.
47. Bermúdez, H., D. A. Hammer, and D. E. Discher. 2004. Effect of bilayer thickness on membrane bending rigidity. *Langmuir.* 20:540–543.

48. Pécréaux, J., H. G. Döbereiner, …, P. Bassereau. 2004. Refined contour analysis of giant unilamellar vesicles. *Eur. Phys. J. E Soft Matter.* 13:277–290.

49. Pan, J., S. Tristram-Nagle, and J. F. Nagle. 2009. Effect of cholesterol on structural and mechanical properties of membranes depends on lipid chain saturation. *Phys. Rev. E Stat. Nonlin. Soft Matter Phys.* 80:021931.

50. Quehenberger, O., A. M. Armando, …, E. A. Dennis. 2010. Lipidomics reveals a remarkable diversity of lipids in human plasma. *J. Lipid Res.* 51:3299–3305.

51. Sampaio, J. L., M. J. Gerl, …, A. Shevchenko. 2011. Membrane lipidome of an epithelial cell line. *Proc. Natl. Acad. Sci. USA.* 108: 1903–1907.

52. van Meer, G., D. R. Voelker, and G. W. Feigenson. 2008. Membrane lipids: where they are and how they behave. *Nat. Rev. Mol. Cell Biol.* 9:112–124.

53. Evans, E., and W. Rawicz. 1990. Entropy-driven tension and bending elasticity in condensed-fluid membranes. *Phys. Rev. Lett.* 64:2094–2097.

54. Khelashvili, G., B. Kollmitzer, …, D. Harries. 2013. Calculating the bending modulus for multicomponent lipid membranes in different thermodynamic phases. *J. Chem. Theory Comput.* 9:3866–3871.

55. Semrau, S., T. Idema, …, C. Storm. 2008. Accurate determination of elastic parameters for multicomponent membranes. *Phys. Rev. Lett.* 100:088101.

56. Pan, J., S. Tristram-Nagle, …, J. F. Nagle. 2008. Temperature dependence of structure, bending rigidity, and bilayer interactions of dioleoylphosphatidylcholine bilayers. *Biophys. J.* 94:117–124.

57. Henriksen, J., A. C. Rowat, and J. H. Ipsen. 2004. Vesicle fluctuation analysis of the effects of sterols on membrane bending rigidity. *Eur. Biophys. J.* 33:732–741.

58. Sengupta, P., A. Hammond, …, B. Baird. 2008. Structural determinants for partitioning of lipids and proteins between coexisting fluid phases in giant plasma membrane vesicles. *Biochim. Biophys. Acta.* 1778: 20–32.

59. Sevcsik, E., M. Brameshuber, …, G. J. Schütz. 2015. GPI-anchored proteins do not reside in ordered domains in the live cell plasma membrane. *Nat. Commun.* 6:6969.

60. Kahya, N., D. A. Brown, and P. Schwille. 2005. Raft partitioning and dynamic behavior of human placental alkaline phosphatase in giant unilamellar vesicles. *Biochemistry.* 44:7479–7489.

61. Levental, I., D. Lingwood, …, K. Simons. 2010. Palmitoylation regulates raft affinity for the majority of integral raft proteins. *Proc. Natl. Acad. Sci. USA.* 107:22050–22054.

62. Dupuy, A. D., and D. M. Engelman. 2008. Protein area occupancy at the center of the red blood cell membrane. *Proc. Natl. Acad. Sci. USA.* 105:2848–2852.

63. Sheetz, M. P. 1993. Glycoprotein motility and dynamic domains in fluid plasma membranes. *Annu. Rev. Biophys. Biomol. Struct.* 22:417–431.

64. Ackerman, D. G., and G. W. Feigenson. 2016. Effects of transmembrane α-helix length and concentration on phase behavior in four-component lipid mixtures: a molecular dynamics study. *J. Phys. Chem. B.* 120:4064–4077.

65. Bloom, M., E. Evans, and O. G. Mouritsen. 1991. Physical properties of the fluid lipid-bilayer component of cell membranes: a perspective. *Q. Rev. Biophys.* 24:293–397.

Biophysical Journal, Volume *114*

Supplemental Information

Membrane Bending Moduli of Coexisting Liquid Phases Containing Transmembrane Peptide

Rebecca D. Usery, Thais A. Enoki, Sanjula P. Wickramasinghe, V.P. Nguyen, David G. Ackerman, Denise V. Greathouse, Roger E. Koeppe, Francisco N. Barrera, and Gerald W. Feigenson

Supporting Material

Bending modulus measurement- additional information

Bending modulus measurements were carried out with fluctuation analysis as in (1) implemented in Matlab version 2014b.

To ensure the harvested GUVs were slightly flaccid for fluctuation analysis, an osmolality difference between the sucrose and glucose solutions of 4 - 5 mOsmol/kg H_2O was ensured with the use of an osmometer (Model 5004, Precision Systems Inc., Natick, MA). GUVs were formed in 97 mM sucrose solution and harvested into 101 mM glucose solution. Due to the density difference and potential distortion by gravity, we limited the size of vesicles to those having radii less than 20 μm (2).

Sample chambers for observation consisted of a no. 1.5 coverslip and traditional microscope slide separated with a silicone spacer (Sigma-Aldrich, St. Louis, MO) of 0.25 mm thickness. All observations took place at room temperature of ~ 23°C. 0.02 mol% C12:0 DiI was included in GUV preparations and fluorescence intensity was used to exclude any vesicles having more than one bilayer (3).

Datasets consisted of 1600 1 ms exposures. Contours were defined using Canny edge detection with $\sigma = 2$ in images with a pixel size of 79 nm. To ensure the contours were approximately circular the ratio of enclosed area to total perimeter is compared to the approximate radius in each frame. We excluded frames in which the contour reflected a change in radii greater than 10% compared to previous frames.

Compositions for Bending Measurements

In Fig. S1, the compositions for each of the four ternary mixtures used in this study are depicted on diagrams with their respective two-phase regions as defined by previous work (4, 5).

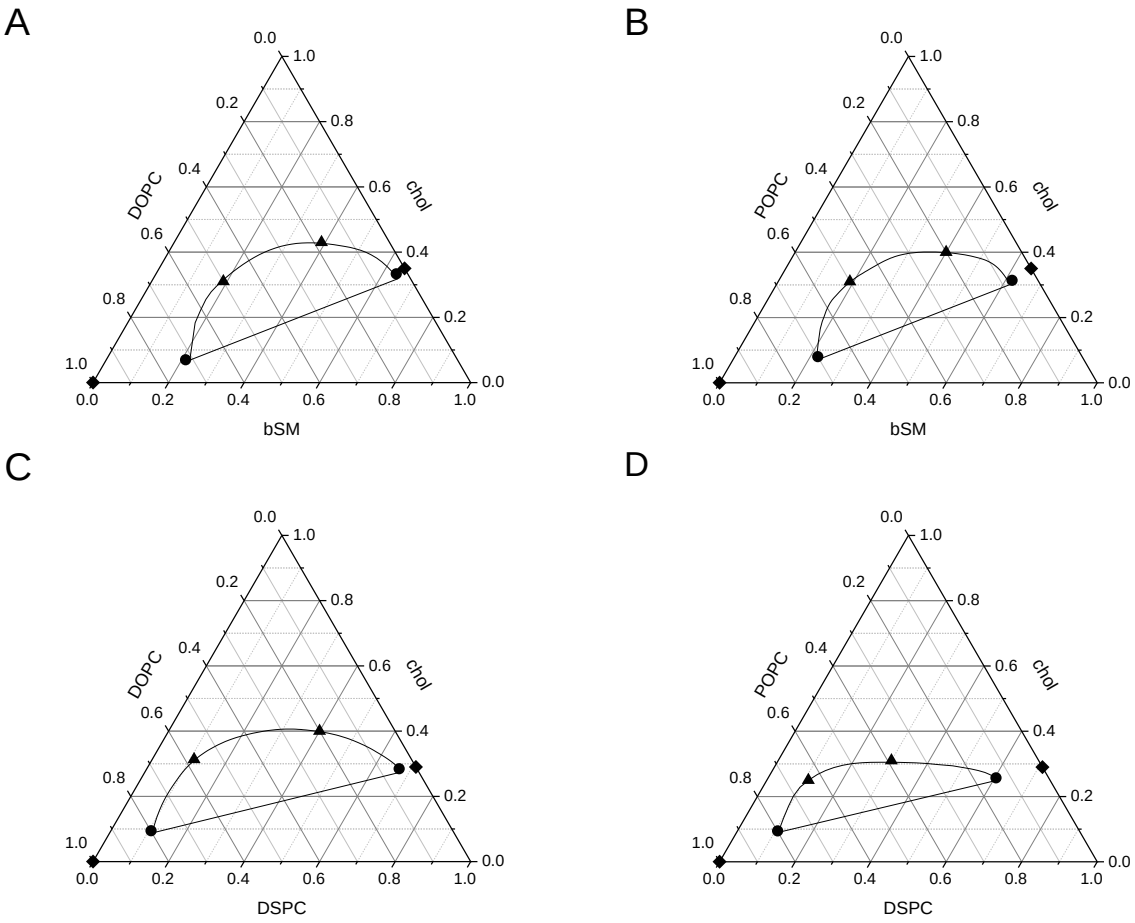

FIGURE S1 Compositions used for bending moduli measurements. The ternary mixtures examined in this work include bSM/DOPC/chol (A), bSM/POPC/chol (B), DSPC/DOPC/chol (C), and DSPC/POPC/chol (D). For each, the simplified (♦), lower tieline endpoint (●), and high cholesterol tieline endpoint (▲) compositions are shown.

Parameters for FRET measurements

FRET along compositional trajectories was used to determine phase boundaries as previously described (6, 5, 4). Partition coefficients were also determined by these means and fitting the experimental data was done as described in the main text. In the FRET experiments, the fluorescence of each dye individually is monitored. The excitation and emission wavelengths for the probes used in this study are detailed in Table S1. The FRET pairs used in this work and corresponding emission and excitation wavelengths monitored are described in Table S2.

Probe	λ_{ex}	λ_{em}
Trp	284	335
DHE	327	393
FAST DiO	477	503
BODIPY-PC	500	520

TABLE S1 Emission (λ_{ex}) and excitation (λ_{em}) wavelengths for individual dye fluorescence.

Donor	**Acceptor**	λ_{ex}	λ_{em}
Trp	DHE	284	393
Trp	BODIPY-PC	284	520
DHE	FAST DiO	327	503
DHE	BODIPY-PC	327	520

TABLE S2 Emission (λ_{ex}) and excitation (λ_{em}) wavelengths for FRET pairs used in this study.

GWALP23 K_p in nanoscopic mixtures

We prepared sample trajectories parallel to the lower tieline for the nanoscopic mixtures, DSPC/POPC/chol and bSM/POPC/chol. FRET from GWALP23 tryptophan to BODIPY-PC is shown in Fig. S2. Though the best fit solid lines indicate K_p of the peptide is 4 ± 1 and 3 ± 1 in DSPC/POPC/chol and bSM/POPC/chol, respectively, the actual preference of the peptide for Ld would be larger than this fitting suggests because domain size is near the magnitude of the Förster Radius, Ro.

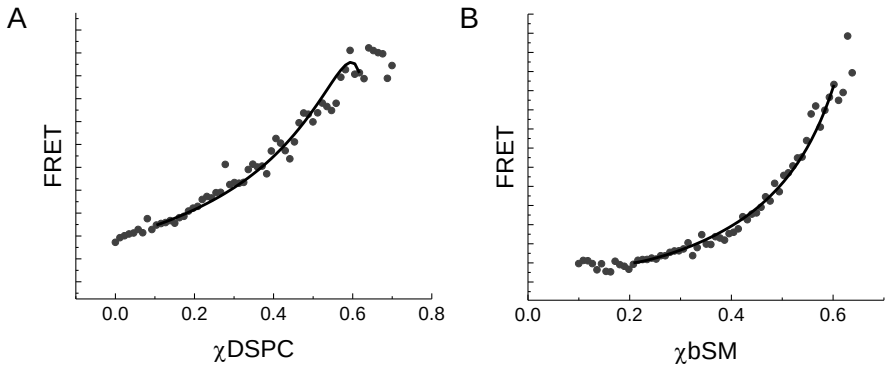

FIGURE S2 GWALP23 partitions into the Ld phase of mixtures with coexisting nanoscopic Ld + Lo domains. (A) FRET (solid circles, AU) from the GWALP23 tryptophan to BODIPY-PC is plotted with respect to DSPC fraction along the trajectory for DSPC/POPC/chol shown in Fig. 1A. The best fit (solid line) to Eq. 2 yields $K_p = 4 \pm 1$. (B) FRET (solid circles, AU) from the GWALP23 tryptophan to BODIPY-PC is plotted with respect to bSM fraction along a trajectory parallel to the lower tieline of the two-phase region for bSM/POPC/chol (4) analogous to that shown in Fig. 1A. The best fit (solid line) to Eq. 2 yields $K_p = 3 \pm 1$. Trajectories included 0.5 mol% GWALP23.

C12:0 DiI Fluorescence calibration

GUV preparations included 0.1 mol% C12:0 DiI. The sample size was varied and lipid concentration was determined by phosphate assay (7). We collected the fluorescence of C12:0 DiI (547/565 ex/em) for these samples. As anticipated, the steady state fluorescence of C12:0 DiI included at a fixed fraction is directly proportional to the lipid concentration, Fig. S3. Thus, the ratio of GWALP23 Trp fluorescence to C12:0 DiI fluorescence is indicative of the protein:lipid ratio in GUV preparations.

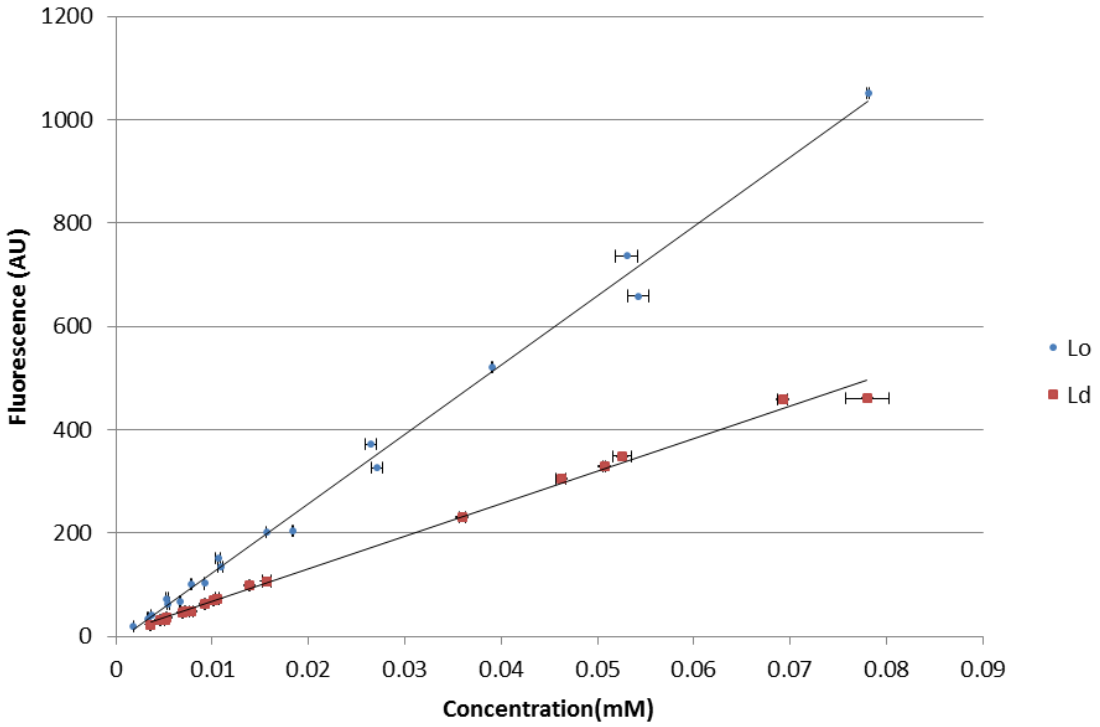

FIGURE S3 C12:0 DiI fluorescence is directly proportional to the lipid concentration. C12:0 DiI fluorescence in Ld (red squares) and Lo (blue circles) is plotted with respect to lipid concentration.

EPR experiments

In an effort to understand how GWALP23 affects membrane lipids, we also conducted EPR experiments using 7PC and 16PC probes. EPR spectra are shown in Fig. S4, and the data is summarized in Table S3. We find the peptide did not significantly affect order along the acyl chains in DSPC/DOPC/chol for Ld. the order and the rate of motion of the acyl chains in Ld did not change in the presence of up to 4 mol% GWALP23. This implies that the significant increase in the bending modulus was not caused by a significant change in the material properties of each leaflet of Ld.

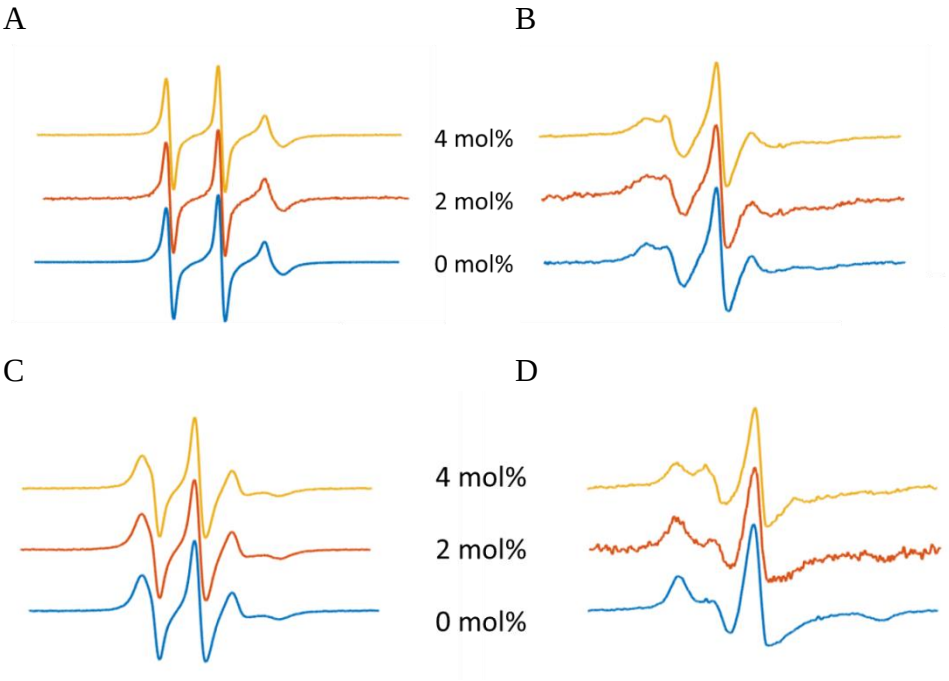

FIGURE S4 EPR spectra for Ld (A, B) and Lo (C, D) with 16:0-16 Doxyl PC (A, C) and 16:0-7Doxyl PC (B, D) with 0 (blue), 2 (orange), and 4 (yellow) mol% WALP23.

spin label	GWALP23 (mol%)	S_{Ld}	S_{Lo}
16 Doxyl PC	0	0.13	0.33
	2	0.12	
	4	0.13	
7 Doxyl PC	0	0.29	0.41
	2	0.28	
	4	0.29	

TABLE S3. DSPC/DOPC/chol Ld and Lo order parameters (S_{Ld} and S_{Lo}, respectively) with 0, 2, and 4 mol% GWALP23. Order parameter for Lo with GWALP23 not depicted based on OCD experiments.

Partitioning of FAST DiO at high- and low-cholesterol

For the mixture DSPC/DOPC/chol, we determined the partition coefficient of FAST DiO between Ld and Lo at low and high cholesterol content. The K_p of FAST DiO is 12 ± 2 at low cholesterol content and 4 ± 1 at high cholesterol content, Fig. S5. This change in K_p mirrors the change in K_p observed for GWALP23, Figs 2A and 7.

A B

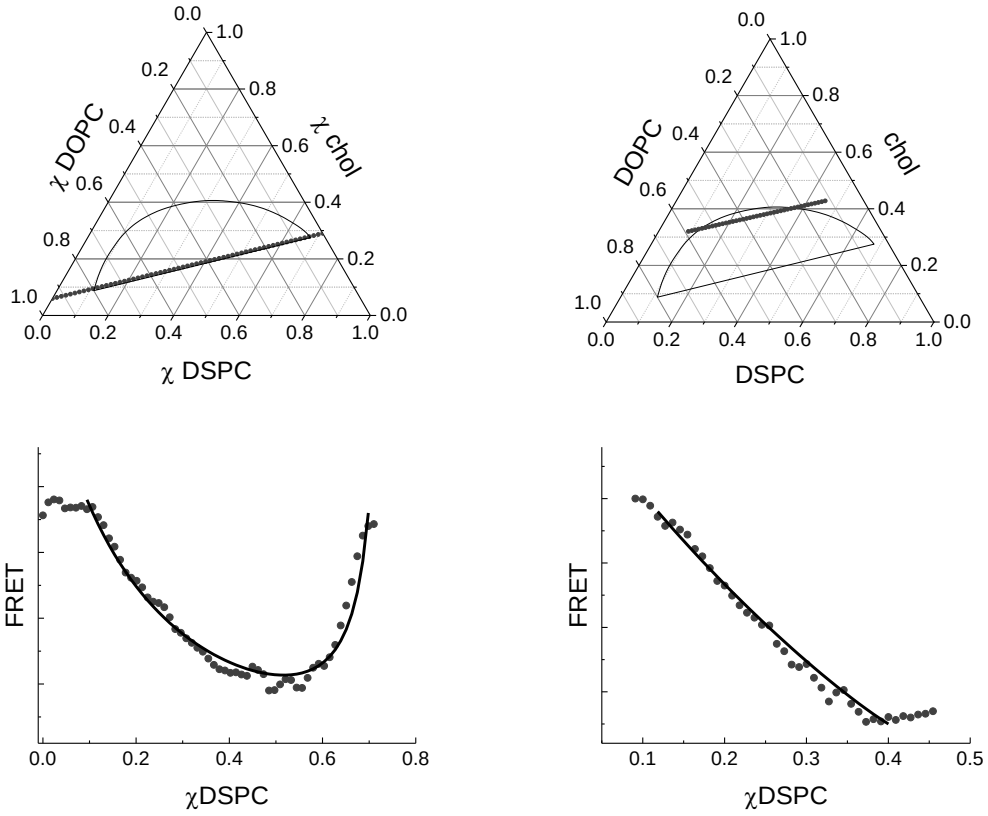

FIGURE S5 FAST DiO K_p decreases with increased cholesterol content. (A) Diagram showing the sample compositions used in low-cholesterol trajectory coinciding with the lower tieline of the two-phase region. Intensity of FRET from DHE to FAST DiO along the trajectory is shown in the lower panel. The best fit of the experimental data (solid line) yields K_p = 12 ± 2. (B) Diagram illustrating the compositional space traversed by the high-cholesterol trajectory and the phase coexistence region (Ld+Lo) for DSPC/DOPC/chol. Lower panel shows the intensity of FRET from DHE to FAST DiO. The best fit of the experimental data (solid line) yields K_p = 4 ± 1.

Bending modulus of DOPC + GWALP23

For comparison to the ternary mixtures, we measured the bending modulus of a simplified Ld phase, DOPC, with peptide. Like the ternary Ld phases, the bending modulus increased with peptide concentration, but the increase was more gradual. For this simplified Ld phase, GUV yield could be maintained with a higher fraction of peptide.

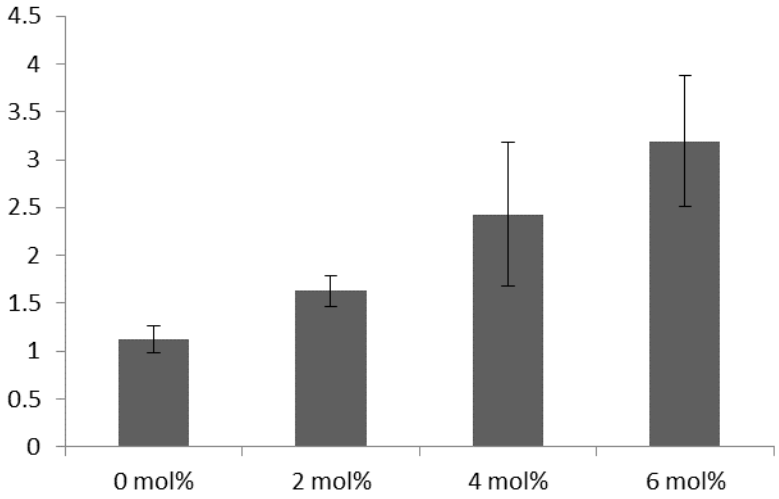

FIGURE S6 GWALP23 increases the membrane bending rigidity of the DOPC membranes. Bending moduli, κ, in 10^{-19} J of DOPC with 0, 2, 4, and 6 mol% GWALP23.

References

1. Usery, R.D., T.A. Enoki, S.P. Wickramasinghe, M.D. Weiner, W.-C. Tsai, M.B. Kim, S. Wang, T.L. Torng, D.G. Ackerman, F.A. Heberle, J. Katsaras, and G.W. Feigenson. 2017. Line Tension Controls Liquid-Disordered + Liquid-Ordered Domain Size Transition in Lipid Bilayers. Biophys. J. 112: 1431–1443.

2. Henriksen, J.R., and J.H. Ipsen. 2002. Thermal undulations of quasi-spherical vesicles stabilized by gravity. Eur. Phys. J. E. Soft Matter. 9: 365–74.

3. Akashi, K., H. Miyata, H. Itoh, and K. Kinosita. 1996. Preparation of giant liposomes in physiological conditions and their characterization under an optical microscope. Biophys. J. 71: 3242–50.

4. Petruzielo, R.S., F.A. Heberle, P. Drazba, J. Katsaras, and G.W. Feigenson. 2013. Phase behavior and domain size in sphingomyelin-containing lipid bilayers. Biochim. Biophys. Acta. 1828: 1302–13.

5. Konyakhina, T.M., J. Wu, J.D. Mastroianni, F.A. Heberle, and G.W. Feigenson. 2013. Phase diagram of a 4-component lipid mixture: DSPC/DOPC/POPC/chol. Biochim. Biophys. Acta. 1828: 2204–14.

6. Zhao, J., J. Wu, F. a Heberle, T.T. Mills, P. Klawitter, G. Huang, G. Costanza, and G.W. Feigenson. 2007. Phase studies of model biomembranes: complex behavior of DSPC/DOPC/cholesterol. Biochim. Biophys. Acta. 1768: 2764–76.

7. Kingsley, P. B., Feigenson, G.W. 1979. The Synthesis of a Perdueterated Phospholipid: 1,2-dimyristoyl-sn-glycero-3-phosphocholine-d72. Chem. Phys. Lipids. 24: 135–147.